

# ULTRACAM observations of the black hole X-ray transient XTE J1118+480 in quiescence.

T. Shahbaz,<sup>1\*</sup> V.S. Dhillon<sup>2</sup>, T.R. Marsh<sup>3</sup>, J. Casares<sup>1</sup>, C. Zurita<sup>4</sup>, P.A. Charles<sup>5</sup>,  
C. A. Haswell<sup>6</sup>, R.I. Hynes<sup>7</sup>

<sup>1</sup>*Instituto de Astrofísica de Canarias, 38200 La Laguna, Tenerife, Spain*

<sup>2</sup>*Department of Physics and Astronomy, University of Sheffield, Sheffield, S3 7RH, UK*

<sup>3</sup>*Department of Physics, University of Warwick, Coventry CV4 7AL, England*

<sup>4</sup>*Observatorio Astronómico de Lisboa, Tapada da Ajuda 1349-018, Lisboa, Portugal*

<sup>5</sup>*South African Astronomical Observatory, P.O. Box 9, Observatory, 7935, South Africa*

<sup>6</sup>*Department of Physics and Astronomy, The Open University, Walton Hall, Milton Keynes, MK7 6AA, UK*

<sup>7</sup>*Department of Physics and Astronomy, Louisiana State University, Baton Rouge, LA 70803-4001, USA*

26 November 2018

## ABSTRACT

We present high time-resolution multicolour observations of the quiescent soft X-ray transient XTE J1118+480 obtained with ULTRACAM. Superimposed on the double-humped continuum  $g'$  and  $i'$ -band lightcurves are rapid flare events which typically last a few minutes. The power density spectrum of the lightcurves can be described by a broken power-law model with a break frequency at  $\sim 2$  mHz or a power-law model plus a broad quasi-periodic oscillation (QPO) at  $\sim 2$  mHz. In the context of the cellular-automaton we estimate the size of the quiescent advection-dominated flow (ADAF) region to be  $\sim 10^4$  Schwarzschild radii, similar to that observed in other quiescent black hole X-ray transients, suggesting the same underlying physics. The similarities between the low/hard and quiescent state PDS suggest a similar origin for the optical and X-ray variability, most likely from regions at/near the ADAF.

**Key words:** accretion, accretion disc – binaries: close – stars: individual: XTE J1118+480

## 1 INTRODUCTION

X-ray transients (XRTs) are a subset of low-mass X-ray binaries (LMXBs) that display episodic, dramatic X-ray and optical outbursts, usually lasting for several months. More than 70 percent of XRTs are thought to contain black holes (Charles & Coe 2003).

The XRT XTE J1118+480 was discovered by the *RXTE* All Sky Monitor on 2000 March 29 (Remillard et al. 2000). Given its very high Galactic latitude ( $b = +62$  degrees) and correspondingly low interstellar absorption ( $N_H \sim 1.2 \times 10^{20} \text{ cm}^{-2}$ ), it was possible to observe the multi-wavelength spectrum including the soft X-ray and extreme ultraviolet during outburst (Hynes et al. 2000; McClintock et al. 2001; Chaty et al. 2003). Throughout this time, XTE J1118+480 remained in the low/hard state, characteristic of an accreting black hole binary. A power-law spectrum with an index of -1.7 was seen extending out to 120 keV (Wilson & McCollough 2000; Frontera et al. 2001) with a

similar spectral index to Cyg X-1 in the low/hard state (Remillard et al. 2000). Faint associated radio emission was detected at 6.2 mJy and interpreted in terms of a steady radio jet (Fender et al. 2001).

A 13th magnitude optical counterpart was promptly identified (Uemura, Kato & Yamaoka 2001) and its optical spectrum was typical of a black hole X-ray transient in outburst (Garcia et al. 2000). A 4.1 hr weak optical photometric modulation was discovered (Cook et al. 2000), most likely due to superhumps, i.e. disc precession (Uemura et al., 2002). By late November 2000, XTE J1118+480 was nearly in quiescence and optical radial velocity studies led to the determination of the large binary mass function,  $f(M) = 6.1 \pm 0.3 M_\odot$ , thereby establishing that the compact object is a black hole (Wagner et al. 2001; McClintock et al. 2001; Torres et al. 2004). XTE J1118+480 has the shortest known orbital period for an XRT of 4.08 hr (Zurita et al. 2002), the spectral type of the secondary star is approximately K5V (Wagner et al. 2001; McClintock et al. 2001; McClintock et al. 2003) and the binary inclination

\* E-mail: tsh@ll.iac.es

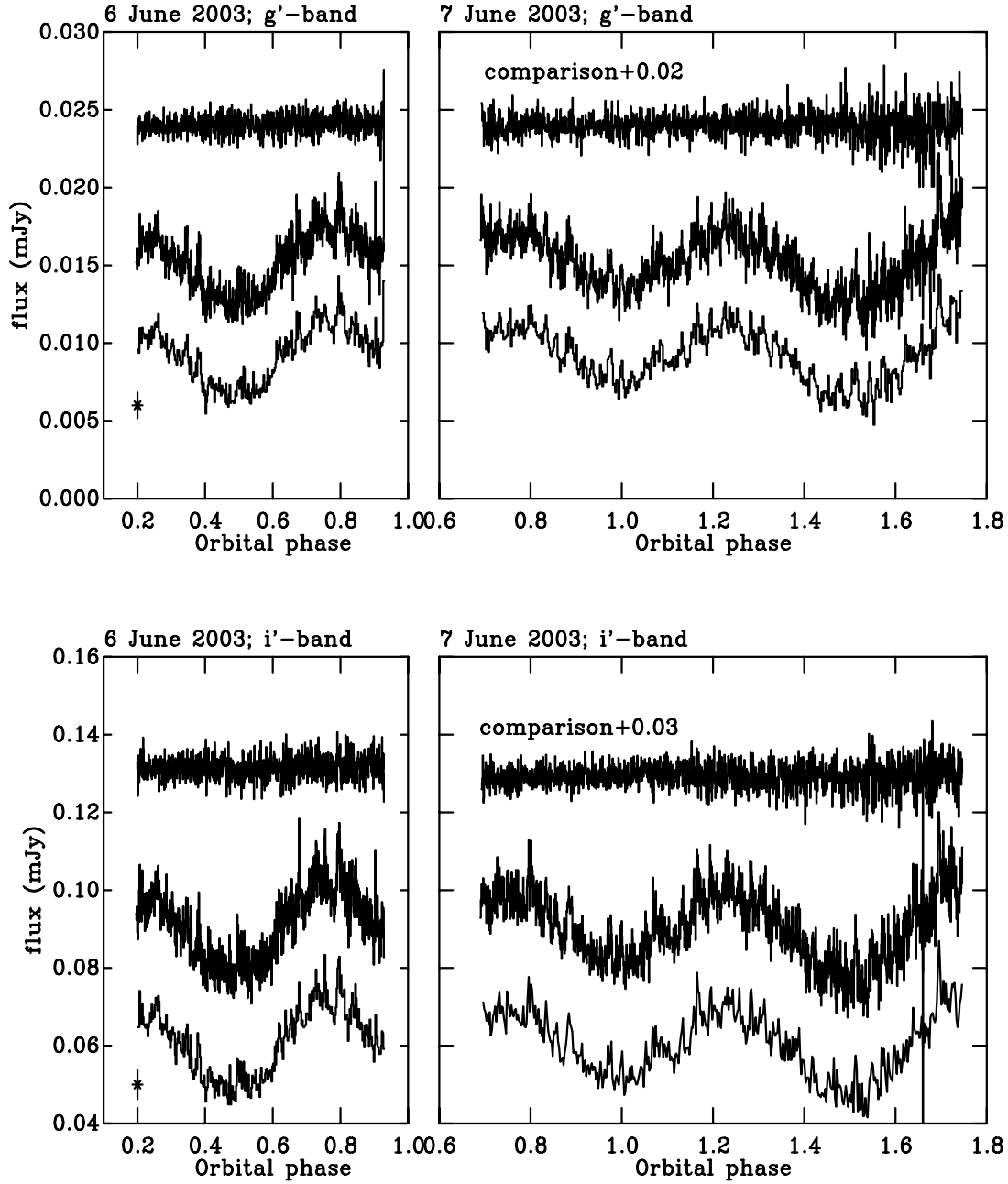


**Figure 1a.** The de-reddened “slow”  $g'$  (top panel) and  $i'$ -band (bottom panel) lightcurves of XTE J1118+480, phase-folded using the ephemeris given in McClintock et al. (2003); phase 0.0 is defined as inferior conjunction of the secondary star. The asterisk marks the typical uncertainty in the data. In order to show the short-term flare more clearly, we also show the lightcurve binned to a time-resolution of 35 s. In each panel we also show the lightcurve of a comparison star of similar magnitude to XTE J1118+480.

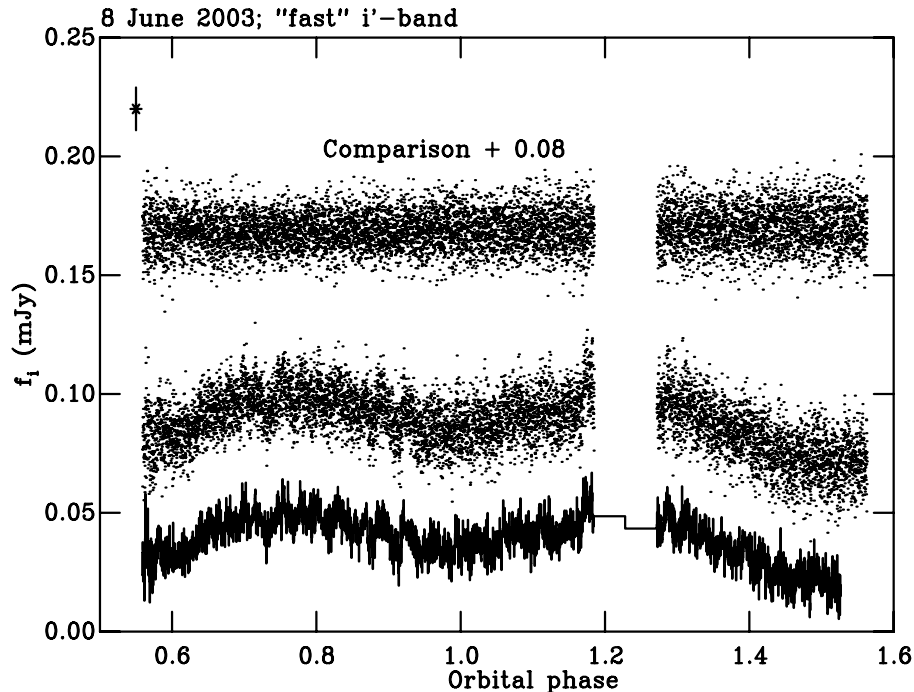


**Figure 1b.** The de-reddened phase-folded “fast”  $i'$ -band lightcurve of XTE J1118+480 (bottom). In order to show the short-term flare more clearly, we also show the lightcurve binned to a time-resolution of 5 s. The asterisk marks the typical uncertainty in the data. The top lightcurve is of a comparison star of similar magnitude to XTE J1118+480.

of the system is high,  $i \sim 80$  degrees (Wagner et al. 2001; Zurita et al. 2002).

Black hole X-ray transients are known to exhibit five distinct X-ray spectral states, distinguished by the presence or absence of a soft blackbody component at 1 keV and the luminosity and spectral slope of emission at harder energies; the quiescent, low, intermediate, high and very high state (Tanaka & Shibazaki 1996). Four of them are successfully explained with the advection dominated accretion flow (ADAF) model (Narayan, McClintock & Yi 1996; Esin, McClintock & Narayan 1997). In the context of the ADAF model, properties similar to the low/hard state are expected for the quiescent state, as there is no distinction between the two except that the mass accretion rate is much higher and the size of the ADAF region is smaller for the former state.

Unlike the transition between the low/hard and high/soft (thermal-dominant) state, where there is a re-configuration of the accretion flow (Esin et al. 1997), there is no observational evidence for a transition between the low/hard and quiescent states. In both these states, the ADAF model predicts that the inner edge of the disc is truncated at some large radius, with the interior region filled by an ADAF. Strong evidence for such a truncated disc is provided by observations of XTE J1118+480 in the low/hard state during outburst (Hynes et al. 2000; McClintock et al. 2001; Esin et al. 2001; Chaty et al. 2003), where the disc has an inner radius of  $>55$  Schwarzschild radii ( $R_{\text{sch}}$ ) and a hot optically-thin plasma in the inner regions. With XTE J1118+480 now in quiescence, the ADAF model predicts that the inner disc edge will move outward to larger radii (Esin et al. 1997). Indeed, McClintock et al.

(2003) recently fit the X-ray/UV/optical quiescent spectrum of XTE J1118+480 and found that it has a hard X-ray spectrum with a spectral photon index of  $\sim 2$ , and an optical/UV continuum that resembles a 13,000 K blackbody disc spectrum with several strong emission lines superimposed. They presented a two-component accretion flow model, an interior region where the flow is advection-dominated and emits in X-rays, and an exterior accretion disc truncated at a transition radius of  $R_{\text{tr}} \sim 10^4 R_{\text{sch}}$  that is responsible for most of the optical/UV spectrum.

Here we report on our high-time resolution multi-colour optical observations of XTE J1118+480 in quiescence. We determine the quiescent PDS, compare it to the X-ray low/hard state PDS and determine the size of the ADAF region in quiescence. These observations are part of a continuous campaign with ULTRACAM to obtain high-time resolution photometry of X-ray binaries.

## 2 OBSERVATIONS AND DATA REDUCTION

Multi-colour photometric observations of XTE J1118+480 were obtained with ULTRACAM on the 4.2-m William Herschel Telescope atop La Palma during the period 2003 June 6 to 8. ULTRACAM is an ultra-fast, triple-beam CCD camera, where the light is split into three broad-band colours (blue, green and red) by two dichroics. The detectors are back-illuminated, thinned, E2V frame-transfer  $1024 \times 1024$  CCDs with a pixel scale of 0.3 arcsecs/pixel. Due to the architecture of the CCDs the dead-time is essentially zero (for further details see Dhillon & Marsh 2001).

**Table 1.** Properties of the flares.  $v_{obs}$  is the spectroscopic veiling,  $v'_d$  is the contribution to the *non-variable* disc light,  $\bar{z}_f$  and  $\sigma_z$  are the mean flare flux and its standard deviation respectively.  $\sigma_z^* = \sigma_z/v'_d$  and  $\eta$  is the fraction of the average veiling due to the flares (Zurita et al. 2003).

band	$v_{obs}$	$v'_d$	$\bar{z}_f$	$\sigma_z$	$\sigma_z^*$	$\eta$
$g'$	40% <sup>1</sup>	39.9%	0.0007	0.0011	0.0027	0.2%
$i'$	-	-	0.0036	0.0050	-	-

<sup>1</sup> Torres et al. (2004)

Our observations were taken using the Sloan  $u'$ ,  $g'$  and  $i'$  filters with effective wavelengths of 3550 Å, 4750 Å and 7650 Å respectively. For the first 2 nights (June 6 to 7), we used an exposure time of 11.65 s, which was sufficient to give reasonable count rates in the  $g'$  and  $i'$  bands. Given the faintness of the object ( $V=19.5$ ) and the short exposure times, few counts were obtained in the  $u'$  band. On the last night (June 8) we decreased the exposure time to 1.65 s, but only data in the  $i'$  band were usable. Hereafter, we will refer to the data taken with exposure times of 11.65 s and 1.65 s as the “slow” and “fast” data, respectively.

The ULTRACAM pipeline reduction procedures were used to debias and flat-field the data. The same pipeline was also used to obtain lightcurves for XTE J1118+480 and several comparison stars by extracting the counts using aperture photometry. The most reliable results were obtained using a large aperture with a radius of 1.8 arcsec. The count ratio of XTE J1118+480 with respect to the local standard (2.28" North 3.75" East of XTE J1118+480 with similar colour to our target) was then determined. The magnitude of XTE J1118+480 was then obtained using the calibrated magnitude of the local standard. As a check of the photometry and systematics in the reduction procedure, we also extracted lightcurves of a comparison star similar in brightness to the target. The mean  $g'$  and  $i'$  band magnitudes of XTE J1118+480 are 21.00 and 19.04 respectively and the rms are 14% and 11% respectively. We estimate the photometric accuracy to be 7.1 and 5.5 percent for the “slow”  $g'$  and  $i'$  band respectively and 6.0 percent for the “fast”  $i'$  band data.

### 3 THE SHORT-TERM VARIABILITY

It is clear that the optical lightcurve of XTE J1118+480 (Figure 1a, 1b) is dominated by the secondary star’s ellipsoidal, which is not linked to the short-term variability/flares (Zurita, Casares & Shahbaz 2003, Hynes et al. 2003a, Shahbaz et al. 2003b). Therefore if we want to determine the flux of the flares, these “steady” contributions must first be removed from the lightcurves. In order to isolate the short-term variability in each band, we first de-reddened the observed magnitudes using a colour excess of  $E(B-V)=0.017$  (Chaty et al. 2003) and the ratio  $A_V/E(B-V)=3.1$  (Cardelli, Clayton, & Mathis 1989), giving  $g'$  and  $i'$  extinction values of 0.06 and 0.04 mags respectively and then converted the Sloan AB magnitudes to flux density (Fukugita et al. 1996). We then fitted a double sinusoid to the lower-envelope of the lightcurve with peri-

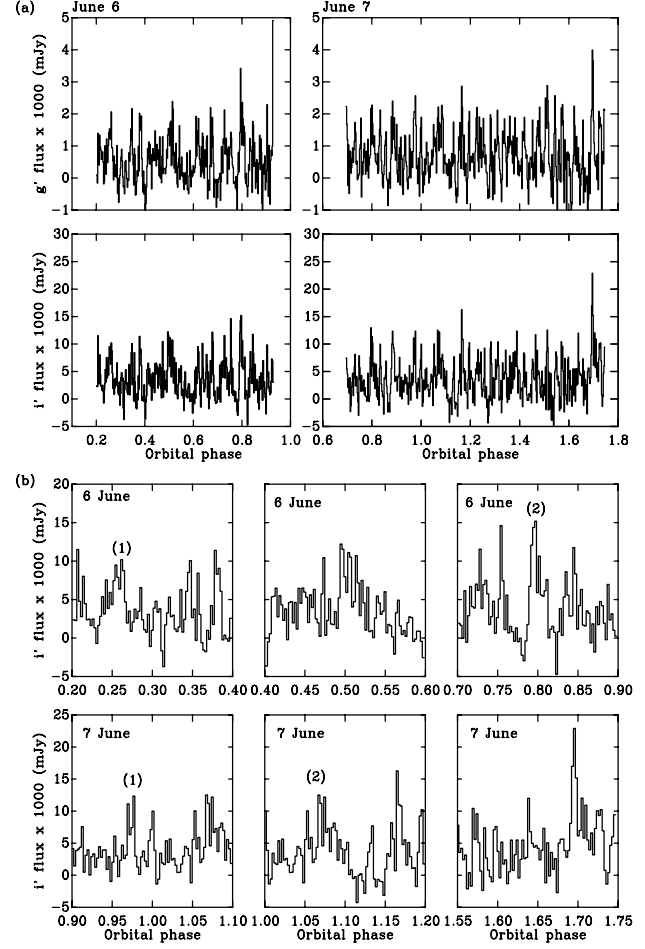


**Figure 2.** (a) The flare de-reddened flux density  $g'$  (top panel) and  $i'$ -band (bottom panel) lightcurves of XTE J1118+480 obtained by subtracting a fit to the lower-envelope of the lightcurves in Figure 1. For clarity, the flare lightcurves have been binned by a factor of 3 (i.e. a time-resolution of 35 s). The uncertainties in the  $g'$  and  $i'$  binned lightcurves are  $3.6 \times 10^{-4}$  mJy and  $1.3 \times 10^{-3}$  mJy, respectively. (b) Detailed plots of some individual flares in the  $i'$ -band lightcurve.

ods equal to the orbital period and its first harmonic, where the phasing was allowed to float free. We rejected points more than  $3\sigma$  above the fit, then refitted, repeating the procedure until no new points were rejected (Zurita et al. 2003; Hynes et al. 2003a). The resulting lightcurves did not show any long-term structure, suggesting that any contamination from a superhump modulation is weak; at the  $<0.50\%$  level. As one can see from Figure 2, there are numerous rapid flare events, which typically last 5 min or less. The parameters of the flares as defined by Zurita et al. (2003) are given in Table 1. Using these flare lightcurves we determined the flux density ratio  $f_{g'}/f_{i'}$  and the equivalent blackbody radius  $R_{BB}$ . To determine the colour temperature corresponding to a given flux density ratio, we integrated blackbody functions with the CCD and Sloan filter response functions and then determined the  $f_{g'}/f_{i'}$  flux density ratio. Given this blackbody temperature we can then determine the corresponding radius of the region that produces the observed de-reddened flux at a distance of 1.7 kpc

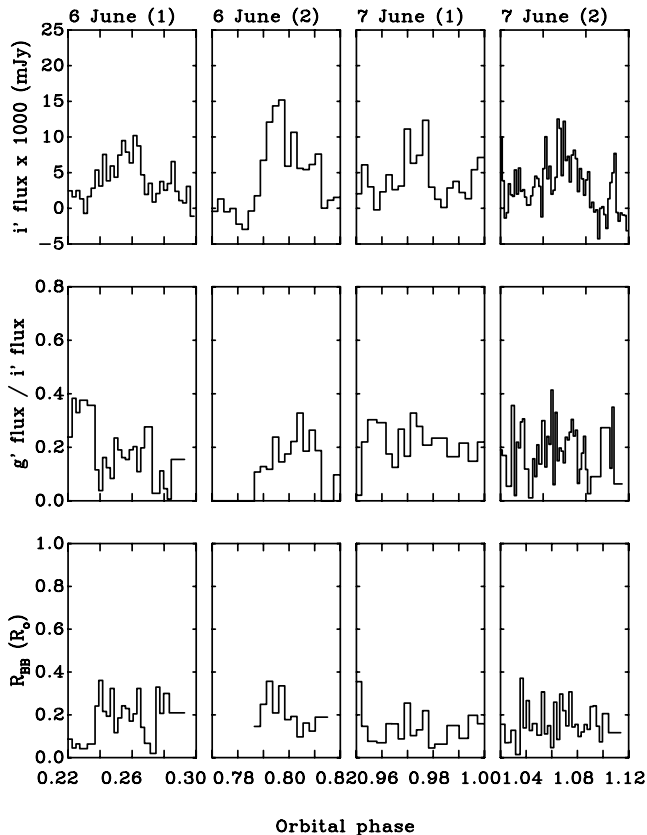


**Figure 3.** In the top panel we show some  $i'$ -band flare profiles shown in Figure 2(b), re-binned by a factor of 3 for clarity. The middle panel shows the flux density ratio  $f_{g'}/f_{i'}$  and the bottom panel shows the projected blackbody radius of the region producing the flares.

(Chaty et al. 2003). Typically, the flares have  $f_{g'}/f_{i'} \sim 0.20$ , similar to the flares in V404 Cyg (Shahbaz et al. 2003b) and  $R_{BB} \sim 0.10 R_{\odot}$ . (see Figure 3). Following the method described in Shahbaz et al. (2003b), we estimate the ratio  $f_{g'}/f_{i'} \sim 0.20 \pm 0.10$  corresponds to a LTE slab of hydrogen with a temperature of  $\sim 3500 \pm 500$  K.

#### 4 THE POWER DENSITY SPECTRUM

To compute the power density spectrum (PDS) of the “slow” and “fast” data, we detrended the data using the double sinusoid fit described in the previous section and then added the mean flux level of the data. Although the ULTRACAM sampling is perfectly uniform, we use the Lomb-Scargle method to compute the periodograms (Press et al. 1992) with the same normalization method as is commonly used in X-ray astronomy, where the power is normalized to the fractional root mean amplitude squared per hertz (van der Klis 1994). We used the constraints imposed by the Nyquist frequency and the typical duration of each observation and binned and fitted the PDS in logarithmic space (Papadakis & Lawrence 1993), where the errors in each bin are determined from the standard deviation of the points within each bin. The white noise level was subtracted by

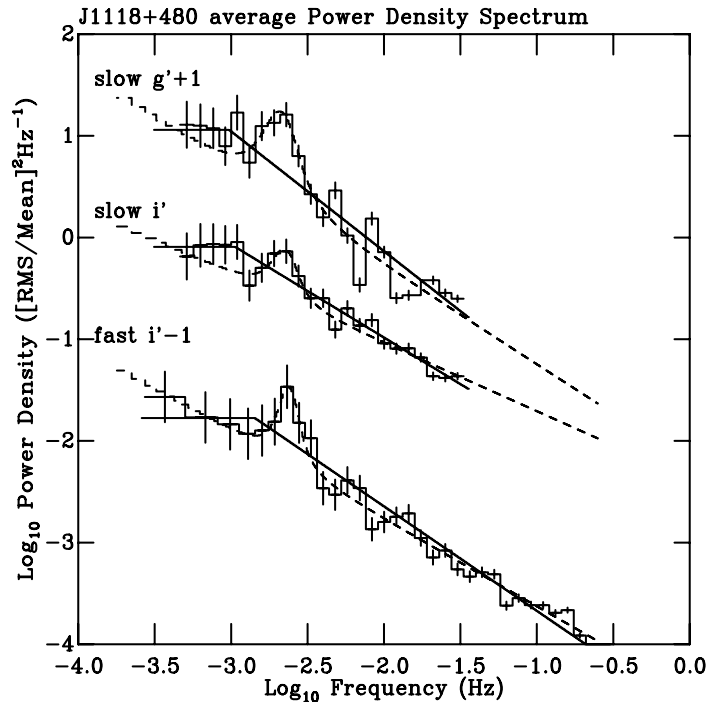


**Figure 4.** The PDS of XTE J1118+480. From top to bottom: “slow”  $g'$  and  $i'$  PDS, and the “fast”  $i'$  PDS. There is a vertical offset between the spectra. The solid line is a fit with a broken power-law and the dashed line is a fit with a power-law+QPO model. A QPO at  $\sim 2$  mHz is noticeable in all the spectra.

fitting the highest frequencies with a white-noise (constant) plus red-noise (power-law) model.

In Figure 4, we show the PDS which can be described by a broken power-law model or a power-law model + quasi-periodic oscillation (QPO). One can see suggestions of a broad QPO in all the PDS, at  $\sim 2$  mHz and/or a break at  $\sim 2$  mHz. Note that the “slow”  $g'$  and  $i'$  PDS are not independent, being simultaneous, but the “fast”  $i'$  is independent, and shows the same (even stronger) feature. Table 2 gives the fitted properties of the PDS. The Q-factor, defined as the centroid frequency divided by the FWHM of the peak in the PDS. Given that the QPO has  $Q > 3$ , in the following sections we will refer to the possible QPO as a “broad QPO”

We tested the significance of the models to describe the PDS using a Monte Carlo simulation similar to Hynes et al. (2003a). We generated lightcurves with exactly the same sampling and integration times as the real data. We started with a model for the ellipsoidal modulation, calculated using the X-ray binary model described in Shahbaz et al. (2003a) with the parameters given in section 3. To this we added a model noise lightcurve generated using a power-law index of  $-1.0$ , a break-frequency at 1 mHz, calculated using the method of Timmer & Koenig (1995), or a broad QPO at 2 mHz with similar strength as observed in the “slow” PDS. We then added Gaussian noise using the errors derived from the photometry. We calculated 1000 simulated lightcurves and analyzed them in exactly the same way as

**Table 2.** Fitted properties of the optical PDS for XTE J1118+480.

PDS	Slope	Break-freq. (mHz)	QPO (mHz)	FWHM (mHz)	rms (%)	Q
“slow” $i'$						
PLB	1.8±0.2	1.9±0.5	-	-	-	-
PL+QPO	1.4±0.2	-	2.2±0.3	0.7±0.8	3.1	3.1
“slow” $g'$						
PLB	2.9±0.3	1.0±0.7	-	-	-	-
PL+QPO	1.9±0.2	-	2.1±0.2	0.8±0.3	5.4	2.6
“fast” $i'$						
PLB	2.3±0.2	1.9±0.3	-	-	-	-
PL+QPO	1.7±0.2	-	2.4±0.4	0.5±1.3	1.9	4.8

\*PL refers to power-law fit of the form  $P \propto \nu^\alpha$ ;

PLB refers to a power-law break and broad QPO refers to a quasi-periodic oscillation;

”rms” refers to the fractional root-mean squared amplitude; ”Q” refers to the quality factor.

for the real data. We created individual PDS with the same logarithmic frequency binning used for the data. With the 1- $\sigma$  confidence levels, we found that the broken power-law and the power-law + QPO model produced a PDS that matched the observations equally (see Figure 5). We therefore conclude that given the uncertainties in the data, the PDS can be described by either the broken power-law or a power-law + broad QPO model.

## 5 THE BREAK FREQUENCY

Most models for the observed optical and X-ray variability from an accretion disc around a black hole [see Wallinder, Kato & Abramowicz (1992) for a review] can produce periodic or quasi-periodic time variations. To reproduce the observed X-ray fluctuations, the physical quantities of the disc must change abruptly and in order to explain the observed 1/f-like fluctuations, a smooth distribution of flares on a variety of time-scales is required. Here we outline the two most attractive mechanisms to produce the 1/f-like fluctuations in X-ray binaries and cataclysmic variables.

### 5.1 The self-organized criticality model

Mineshige, Ouchi & Nishimori (1994a) proposed a cellular-automaton model using the concept of self-organized criticality of Bak, Tang & Wiesenfeld (1988) to explain the observed 1/f-like X-ray fluctuations in X-ray binaries. In their model, the accretion disc comprises of two parts: an outer disc where the disc material smoothly drifts inwards, and an inner disc which suffers an instability. Gas particles are randomly injected into the inner regions of the accretion disc around a black hole. The system then evolves to and stays in a self-organized critical state in spite of random mass injections. Mass accretion occurs either by an avalanche, which is triggered when the mass density of the disc exceeds some critical value, or by gradual gas diffusion (Mineshige, Takeuchi & Nishimori 1994b).

Manmoto et al. (1996) and Takeuchi & Mineshige (1997) took this work further and investigated the response of an advection-dominated disc to an assumed thermal perturbation, producing models in which such X-ray shots could

be continuously created. Since the standard-disc cannot explain the long time-scale of the observed X-ray fluctuations, an advection-dominated disc is favoured, since it is characterized by low-emissivity and a large infall velocity. The main energy release occurs by sporadic reconnection events (Haswell, Tajima & Sakai 1992), leading to magnetic eruptions, similar to solar flares. Magnetic energy is stored and released in an avalanche. They found that the optically thin solutions, dominated by advection (Ichimaru 1977; Narayan & Yi 1994), could produce persistent, but fluctuating hard X-ray emission. Assuming that a disturbance is produced by some critical behavior in the disc, they successfully reproduce the 1/f-like fluctuations at high frequencies and also the break in the PDS at low frequencies, as seen in the PDS of X-ray binaries. The range in frequency over which the 1/f-like fluctuations are observed, depends on the size of the ADAF region of the disc. Beyond the ADAF region (in the outer disc regions), matter accretes smoothly via the usual viscous diffusion process, thus producing white-noise.

The break-frequency is determined by the maximum peak intensity of the X-ray shots which is on the order of the size of the advection-dominated region, and corresponds to the inverse of the free-fall time-scale of the largest avalanches (Takeuchi, Mineshige & Negoro 1995) at the radius of the ADAF region ( $R_{\text{crit}}$ ). As shown in equation 13 of Takeuchi et al. (1995)

$$\frac{R_{\text{crit}}}{R_{\text{sch}}} \sim 10^{3.2} \left( \frac{f_{\text{break}}}{0.1} \right)^{-2/3} \left( \frac{M_{\text{X}}}{10M_{\odot}} \right)^{-2/3} \quad (1)$$

where  $R_{\text{sch}} = 2GM_{\text{X}}/c^2$  is the Schwarzschild radius for a black hole with mass  $M_{\text{X}}$ . However, it should be noted that the break frequency depends not only on the size of the ADAF region but also on the propagation speed of the perturbation (Mineshige priv. comm.). Since the perturbation velocity should be less than the free-fall velocity, the free-fall velocity gives an upper limit to the size of the ADAF. Using  $M_{\text{X}}=7.2M_{\odot}$  and the  $f_{\text{break}} \sim 2$  mHz observed in quiescence (section 4), we find  $R_{\text{crit}} < 3 \times 10^4 R_{\text{sch}} (=0.9 R_{\odot})$ .

### 5.2 The fluctuating viscosity model

Lyubarskii (1997) considered an ADAF disc and showed that

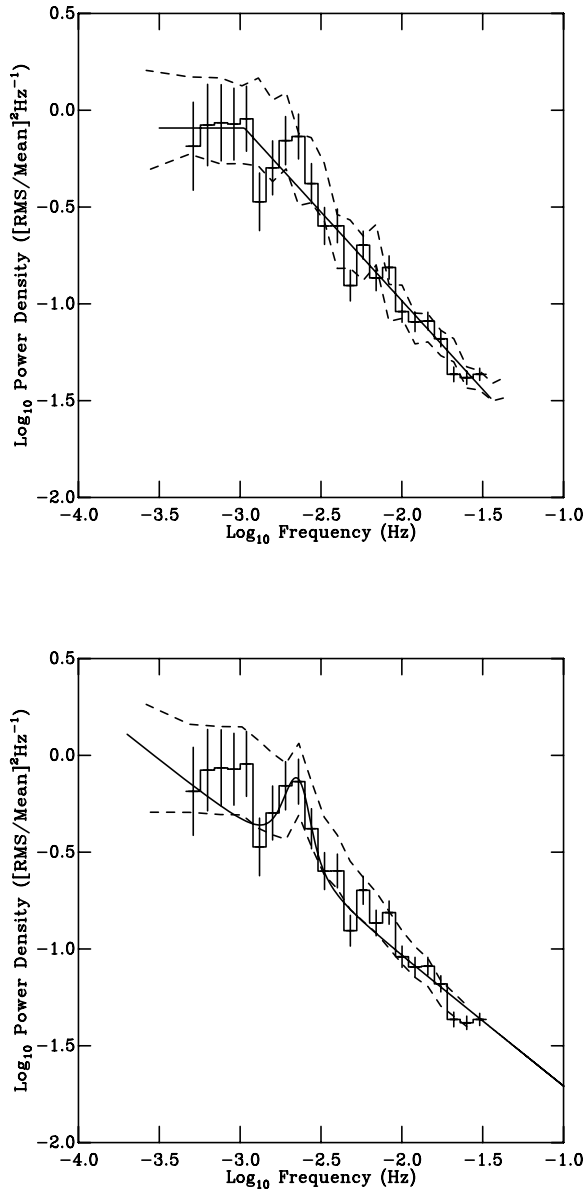


**Figure 5.** Top: The results of the Monte Carlo simulation for a PDS consisting of a broken power-law model. The dotted lines show the 1- $\sigma$  confidence region for individual points obtained by computing 1000 simulations (see text). Bottom: same as above but for a power-law + broad QPO model.

the 1/f-like fluctuations in the accretion rate (and thus luminosity) near the inner radius of the disc can in principle be caused by the viscosity fluctuating independently (most likely due to a magnetic dynamo) at different radii on the local viscous time-scale. Lyubarskii (1997) was able to reproduce a power-law PDS with a frequency break given by the Keplerian accretion time-scale  $\tau = (\alpha\Omega_K^{-1})$ , where  $\Omega_K$  is the Keplerian angular velocity and  $\alpha$  is the dimensionless viscosity parameter (Shakura & Sunyaev 1973). For an observed break-frequency of 2 mHz, this corresponds to an ADAF with an outer disc radius of  $\sim 10^4 R_{\text{sch}}$ .

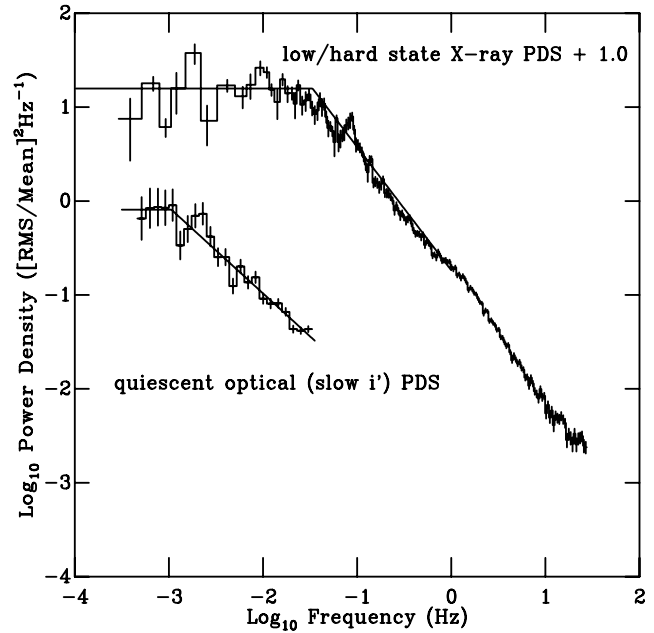


**Figure 6.** The quiescent optical (“slow”  $i'$ ) and low/hard state X-ray PDS of XTE J1118+480 (taken from Hynes et al. 2003b). Note the shift in the break-frequency and broad QPO. The solid lines are broken power-law fits.

Recently, King et al. (2004) have shown how the local magnetic dynamo in the disc can also affect the disc evolution. Angular momentum losses due to a disc wind/jet can significantly drive the accretion rate in systems which are in a jet-dominated state (Fender, Gallo & Jonker 2003). King et al. (2004) consider an accretion disc in which a magnetic dynamo generates the viscosity, but also occasionally produces a well-ordered poloidal field which affects the accretion rate by driving a wind/jet (Livio, Pringle & King 2003). The luminosity arises from viscous dissipation in the disc after allowing for the energy removed by a wind/jet, and produces a 1/f-like PDS and a break-frequency given by the magnetic alignment time-scale at the inner disc edge. However, it should be noted that in their models the disc extends to the last stable orbit around a black hole, as is the case for the X-ray high/soft thermal dominant state. Although this is an attractive model, because in principle the same model could be used to explain the flickering in cataclysmic variables, it is clear that it needs to be adapted to include an ADAF in the low/hard or quiescent states.

## 6 THE LOW-FREQUENCY $\sim 2$ MHz BROAD QPO

During the outburst of XTE J1118+480 a  $\sim 0.08$  Hz QPO was reported in the X-rays (Revnivtsev, Sunyaev & Borozdin 2000) and subsequently confirmed by *ASCA* data (Yamaoka et al. 2000) as well as *RXTE* observations (Wood et al. 2000). Simultaneous *RXTE/HST* observations showed a similar QPO (Haswell et al. 2000) and that the variability in the X-rays

and optical/UV bands were correlated (Hynes et al. 2003b). In Figure 4 there is a suggestion of a broad QPO in the quiescent simultaneous “slow”  $g'$  and  $i'$  PDS and the independent “fast”  $i'$  PDS at  $\sim 2$  mHz.

In the context of a two-component accretion flow model (Narayan et al. 1996; Narayan, Barret & McClintock 1997) an ADAF has turbulent gas at all radii, with a variety of time-scales, ranging from a slow time-scale at the transition radius down to nearly the free-fall time close to the black hole. Interactions between the hot inner ADAF and the cool, outer disc, at or near the transition radius, can be a source of optical QPO variability, due to synchrotron emission by the hot electrons in the ADAF, and would have a characteristic time-scale given by a multiple of the Keplerian rotation period at the transition radius. If we assume that the 2 mHz broad QPO observed in the PDS is the dynamical time-scale at the transition radius, then the transition radius lies at  $\sim 8000 R_{\text{sch}}$ .

## 7 DISCUSSION

Band-limited noise and QPOs are a common feature in the low/hard state XRTs and many LMXBs (McClintock & Remillard 2003). Indeed, observations of XTE J1118+480 in the low/hard state reveal the presence of band-limited noise at X-ray and optical/UV wavelengths (Hynes et al. 2003b). For comparison, in Figure 6 we show the low/hard state X-ray PDS of XTE J1118+480 along with our optical quiescent PDS (section 4). The low/hard state X-ray PDS shows a low-frequency break at 23 mHz and a QPO at  $\sim 80$  mHz, whereas the optical quiescent PDS shows either a break at a much lower frequency of  $\sim 2$  mHz or a broad QPO at  $\sim 2$  mHz. It is interesting to compare the optical and X-ray PDS assuming that the optical PDS can be described by either a break-frequency or a broad QPO model. The position of the quiescent optical broad QPO is a factor of  $\sim 40$  lower than the low/hard state QPO, and the quiescent optical break-frequency is  $\sim 12$  lower than the low/hard state break-frequency. The presence of the possible break-frequency or a broad QPO (possibly with a multiple frequency ratio) provides evidence that we are seeing the same phenomenon in outburst. The similarity between the low/hard and quiescent state PDS suggest that the optical variability could have a similar origin to the X-ray PDS and might be associated with the size of the direct emission from the self-absorbed synchrotron emission arising from an advective-dominated flow (see Narayan & Yi 1994 and references therein) or from optically thin synchrotron emission directly from a jet (Markoff, Falcke & Fender 2001; Fender, Gallo & Jonker 2003). The quiescent state would have a larger ADAF region than in the low/hard state.

The slope of the  $g'$  PDS is steeper than the slope of the  $i'$  PDS, in contrast to what is observed in V404 Cyg (Shahbaz et al. 2003b). This difference could be due to either more low-frequency disc variability in  $g'$  compared to  $i'$  or more high-frequency variability in  $i'$  compared to  $g'$ . The latter would arise if there were more high frequency variability in  $i'$  from the inner disk, such as from the synchrotron emission arising from the ADAF.

The low/hard and quiescent states of the XRTs are often interpreted as having a truncated disc with an ADAF

central region. An ADAF model has been successfully applied to XTE J1118+480 (McClintock et al. 2001; Esin et al. 2001; Chaty et al. 2003). With spectral coverage which includes X-rays, Extreme Ultraviolet (EUV) and radio, model fits to the spectral energy distribution in the low/hard state suggests an ADAF inner radius of  $350 R_{\text{sch}}$  (Chaty et al. 2003). Recently McClintock et al. (2003) have determined the multi-wavelength X-ray/UV/optical quiescent spectrum of XTE J1118+480 and find that the spectrum has two components explained by an ADAF in the disc interior with a radius of  $\sim 10^4 R_{\text{sch}}$ , and an optical/UV continuum that resembles a 13,000 K disc blackbody model spectrum with a radius of  $1500 R_{\text{sch}}$  arising from the disc/stream impact region.

The exterior accretion disc truncated at a radius of  $R_{\text{tr}} \sim 10^4 R_{\text{sch}}$  is responsible for a substantial fraction of the optical/UV spectrum. Although an ADAF of this large size fits the X-ray data it does not produce a significant UV/optical component (Narayan et al. 1997). Furthermore, a significant ADAF contribution to the optical/UV emission is ruled out because of (1) the presence of broad emission lines; (2) the Planckian shape of the optical/UV continuum spectrum, and (3) the large orbital modulation of the NUV continuum which cannot be attributed to synchrotron emission from an ADAF. For the models outlined in sections 5 and 6 we also find a quiescent ADAF radius of  $R_{\text{crit}} \sim 10^4 R_{\text{sch}}$ , comparable to the size of the quiescent ADAF region in the black hole A0620-00 and V404 Cyg, suggesting that the size of the ADAF region is determined by the same underlying physical mechanism, such as viscosity and inner disc temperature.

In section 3 we determined the blackbody colour and radius of the short-term rapid flares. We find that the flares have a blackbody temperature of  $\sim 3500$  K and a radius of  $\sim 0.10 R_{\odot} (= 3200 R_{\text{sch}})$ , which is larger and cooler than the size and temperature of the gas stream/disc impact region determined by McClintock et al. (2003). Most probably the short-term flares arise from *all* regions in the outer parts of the disc. However, it should be noted that Torres et al. (2004) find no evidence for a bright spot (disc/stream impact region) from their optical spectroscopy taken in Jan 2003; a 13,000 K spectrum (McClintock et al. 2003) is not enough to produce Balmer emission lines. It could be that the mass transfer from the secondary star has reduced considerably and so the parameters for the short-term rapid flares we derive could be consistent with an origin from the bright spot. Only high-time resolution spectroscopic observations can resolve this issue.

### 7.1 Quiescent state models

Although the quiescent thermal ADAF model, which predicts a curvature in the X-ray spectrum primarily because of the assumption of a thermal (power-law) energy distribution for the electrons (Esin et al. 1997; Esin et al. 1998), is consistent with the observed X-ray data (McClintock et al. 2003), it should be noted that given the quality of the data, a power-law model as predicted by an ADAF with non-thermal electrons cannot be ruled out. The quiescent optical/UV data suggests a 13,000 K multi-colour blackbody spectrum, arising from the accretion disc and/or where the gas stream impacts the disc. In principle a jet model, such



as the one presented by Markoff, Falcke & Fender (2001) for XTE J1118+480 in the low/hard state, could be modified and applied to the quiescent optical/X-ray data shown in McClintock et al. (2003). Since the jet model is a non-thermal model, one would expect it to predict a power-law spectrum in the X-ray band, which would be consistent with the data.

In the context of a jet model, it could be that the quiescent infrared/optical spectrum of XTE J1118+480 is an extension of the radio spectrum. If the radio spectrum is due to self-absorbed synchrotron emission from a conical jet, then above some frequency (at which the whole jet is optically thin) there should be a break to an optically thin synchrotron spectrum. Observations of the low/hard state X-ray source GX 339-4 appears to have identified such a break in the near-infrared *I*-band (Corbel & Fender 2002). For GX 339-4 the X-ray spectrum seems to lie on an extrapolation of the non-thermal component. Looking at quiescent optical/X-ray SED of XTE J1118+480 (McClintock et al. 2003), it seems difficult to describe the X-ray as a continuation of the optical data. For XTE J1118+480 a similar two-component quiescent SED overlapping in the optical/infrared, with an additional Planckian component due to an accretion disc may be expected, as is indeed predicted by the jet models (Markoff, Falcke & Fender 2001), but it is clear that quiescent data at radio and infrared wavelengths are needed before any firm conclusions can be drawn.

## 8 CONCLUSION

We present ULTRACAM observations of the quiescent soft X-ray transient XTE J1118+480. Superimposed on the *g'* and *i'*-band ellipsoidal lightcurves are rapid flare events, the PDS of which can be described by either a broken power-law model with a break frequency at  $\sim 2$  mHz or a power-law model plus a broad quasi-periodic oscillation (QPO) at  $\sim 2$  mHz. In either case, the size of the quiescent ADAF region is estimated to be  $\sim 10^4$  Schwarzschild radii, similar to that observed in other quiescent black hole X-ray transients. The similarities between that the low/hard state PDS (80 mHz QPO and a  $\sim 23$  mHz break-frequency) with the quiescent state optical PDS suggest a similar origin for the optical and X-ray variability, most likely from regions at/near the ADAF region.

## ACKNOWLEDGMENTS

TS and JC acknowledge support from the Spanish Ministry of Science and Technology under the grant AYA 2002 03570 and the programme Ramón y Cajal. TRM acknowledges the support of a PPARC Senior Research Fellowship. ULTRACAM is supported by PPARC grant PPA/G/S/2002/00092. Based on observations made with the William Herschel Telescope operated on the island of La Palma by the Isaac Newton Group in the Spanish Observatorio del Roque de los Muchachos of the Instituto de Astrofísica de Canarias.

## REFERENCES

- Cardelli J. A., Clayton G. C., Mathis J. S., 1989, *ApJ*, 345, 245
- Charles P. A., Coe M., 2003, in *Compact Stellar X-ray Sources*, eds. W.H.G. Lewin and M. van der Klis, Cambridge University Press, astro-ph/0308020
- Chaty S., Haswell C. A., Malzac J., Hynes R. I., Shrader C. R., Cui W., 2003, *MNRAS*, 346, 689
- Cook L., Patterson J., Buczynski D., Fried R., 2000, *IAUC*, 7397, 2
- Corbel S., Fender R. P., 2002, *ApJ*, 573, L35
- Dhillion V., Marsh T. R., 2001, *NewAR*, 45, 91
- Esin A. A., McClintock J. E., Narayan R., 1997, *ApJ*, 489, 865
- Esin A. A., Narayan R., Cui W., Grove J. E., Zhang S. N., 1998, *ApJ*, 505, 854
- Esin A. A., McClintock J. E., Drake J. J., Garcia M. R., Haswell C. A., Hynes R. I., Munro M. P., 2001, *ApJ*, 555, 483
- Fender R. P., Hjellming R. M., Tilanus R. P. J., Pooley G. G., Deane J. R., Ogley R. N., Spencer R. E., 2001, *MNRAS*, 322, L23
- Fender R. P., Gallo E., Jonker P. G., 2003, *MNRAS*, 343, L99
- Frontera F. et al., 2001, *ApJ*, 561, 1006
- Fukugita M., Ichikawa T., Gunn J. E., Doi M., Shimasaku K., Schneider D. P., 1996, *AJ*, 111, 1748
- Garcia M., Brown W., Pahre M., McClintock J. E., Callanan P., Garnavich P., 2000, *IAUC*, 7392, 2
- Haswell C. A., Tajima Sakai, 1992, *ApJ*, 401, 495
- Haswell C. A., Skillman D., Patterson J., Hynes R. I., Cui W., 2000, *IAUC*, 7427, 1
- Hynes R. I., Mauche C. W., Haswell C. A., Shrader C. R., Cui W., Chaty S., 2000, *ApJ*, 539, L37
- Hynes R. I., Charles P. A., Casares J., Haswell C. A., Zurita C., Shahbaz T., 2003a, *MNRAS*, 340, 447
- Hynes R. I., et al., 2003b, *MNRAS*, 345, 292
- Ichimaru S., 1977, *Ap*, 214, 840
- King A. R., Pringle J. E., West R. G., Livio M., 2004, *MNRAS*, 348, 111
- Livio M., Pringle J. E., King A. R., 2003, *ApJ*, 593, 184
- Lyubarskii Y. E., 1997, *MNRAS*, 292, 679
- McClintock J. E., Garcia M. R., Caldwell N., Falco F. E., Garnavich P. M., Zhao P., 2001a, *ApJ*, 551, L147
- McClintock J. E., et al. 2001b, *ApJ*, 555, 477
- McClintock J. E., Narayan R., Garcia M. R., Orosz J. E., Remillard R. A., Murray S. S. 2003, *ApJ*, 593, 435
- McClintock J. E., Remillard R., 2003, in *Compact Stellar X-ray Sources*, eds. W.H.G. Lewin and M. van der Klis, Cambridge University Press, astro-ph/0306213
- Manmoto T., Takeuchi M., Mineshige S., Matsumoto R., Negoro H., 1996, *ApJ*, 464, L135
- Markoff S., Falcke H., Fender R. P., 2001, *A&A*, 372, L25
- Menou K., Narayan R., Lasota J., 1999, *ApJ*, 513, 811
- Mineshige S., Ouchi N. B., Nishimori H., 1994, *PASJ*, 46, 97
- Mineshige S., Takeuchi M., Nishimori H., 1994, *ApJ*, 435, L125
- Narayan R., Yi I., 1994, *ApJ*, 428, L13
- Narayan R., McClintock J. E., Yi I., 1996, *ApJ*, 457, 821
- Narayan R., Barret D., McClintock J. E., 1997, *ApJ*, 482, 448
- Papadakis I. E., Lawrence A., 1993, *MNRAS*, 261, 612

- Press W. H., Teukolsky S. A., Vetterling W. T., Flannery B. P., 1992, *Numerical Recipes*, 2nd Edn., CUP, Cambridge
- Remillard R., Morgan E., Smith D., Smith E., 2000, *IAUC*, 7389, 2
- Revnivtsev M., Sunyaev R., Borozdin K., 2000, *A&A*, 361, L37
- Shahbaz T., Zurita C., Casares J., Dubus G., Charles P. A., Wagner R. M., Ryan E., 2003a, 585, 443
- Shahbaz T., Dhillon V. S., Marsh T. R., Zurita C., Haswell C. A., Hynes R. I., Charles P. A., Casares J., 2003b, *MNRAS*, 346, 1116
- Shakura N. I., Sunyaev R. A., 1973, *A&A*, 24, 337
- Takeuchi M., Mineshige S., Negoro H., 1995, *PASJ*, 47, 617
- Takeuchi M., Mineshige S., 1997, *ApJ*, 486, 160
- Tanaka Y., Shibasaki N., 1996, *ARA&A*, 34, 607
- Timmer J., Koenig M., 1995, *A&A*, 300, 707
- Torres M. A. P., Callanan P. J., Garcia M. R., Zhao P., Laycock S., Kong A. K. H., 2004, *ApJ*, 612, 1026
- Uemura M., Kato T., Yamaoka H., 2001, *IAUC* #7329
- Uemura M., et al., 2002, *PASJ*, 54, 285
- van der Klis M., 1994, *ApJS*, 92, 511
- Wagner R. M., Foltz C. B., Shahbaz T., Casares J., Charles P. A., Starrfield S. G., Hewett P., 2001, *ApJ*, 556, 42
- Wallinder F. H., Kato S., Abramowicz M. A., 1992, *A&ARv*, 4, 79
- Wilson C. A., McCollough M. L., 2000, *IAUC*, 7390, 3
- Wood K. S., et al., 2000, *ApJ*, 544, L45
- Yamaoka K., Ueda Y., Dotani T., Durouchoux P., Rodriguez J., 2000, *IAUC*, 7427, 2
- Zurita C. et al., 2002, *MNRAS*, 333, 791
- Zurita C., Casares J., Shahbaz T., 2003, *ApJ*, 582, 369